Particle-in-cell with Monte Carlo collision modeling of the electron and negative hydrogen ion transport across a localized transverse magnetic field

St. Kolev,[a] G. J. M. Hagelaar, and J. P. Boeuf
Laboratoire Plasma et Conversion d'Energie (LAPLACE), Université Paul Sabatier, Bt. 3R2, 118 Route de Narbonne, 31062 Toulouse Cedex 9, France

(Received 13 January 2009; accepted 18 February 2009; published online 30 April 2009)

The control of the electron temperature and charged particle transport in negative hydrogen ion sources has a crucial role for the performance of the system. It is usually achieved by the use of a magnetic filter—localized transverse magnetic field, which reduces the electron temperature and enhances the negative ion yield. There are several works in literature on modeling of the magnetic filter effects based on fluid and kinetic modeling, which, however, suggest rather different mechanisms responsible for the electron cooling and particle transport through the filter. Here a kinetic modeling of the problem based on the particle-in-cell with Monte Carlo collisions method is presented. The charged particle transport across a magnetic filter is studied in hydrogen plasmas with and without including volume production of negative ions, in a one-dimensional Cartesian geometry. The simulation shows a classical (collisional) electron diffusion across the magnetic filter with reduction in the electron temperature but no selective effect in electron energy is observed (Coulomb collisions are not considered). When a bias voltage is applied, the plasma is split into an upstream electropositive and a downstream electronegative regions. Different configurations with respect to bias voltage and magnetic field strength are examined and discussed. Although the bias voltage allows negative ion extraction, the results show that volume production of negative ions in the downstream region is not really enhanced by the magnetic filter. © *2009 American Institute of Physics*. [DOI: 10.1063/1.3116650]

I. INTRODUCTION

Current development of large scale fusion reactors [such as ITER (Ref. 1)] has stimulated an intensive research on neutral beam injection systems for fusion plasma heating, based on negative hydrogen ion sources.[2–4] The negative ion production in these sources is due to volume or surface processes, but in both cases the electron temperature and flux needs to be controlled for efficient ion production and extraction. This is usually accomplished by the use of magnetic filtering.

Basically, the filter is a localized magnetic field in the order of few tens of gauss, directed perpendicularly to the plasma flow (Fig. 1). The field is usually produced by an external magnet or by series of small permanent magnets positioned in the vacuum chamber.[3,5,6] The use of magnetic filtering in the sources of negative hydrogen ions was proposed in the beginning of the 1980s (Ref. 7) for controlling the plasma parameters. It was found experimentally[7,8] that the introduction of magnetic filter in the source leads to a significant decrease in the electron temperature (T_e) and increase in the negative ion yield. In this way the filter allows for efficient separation of the power deposition region—the upstream region—and the expansion (downstream) region (Fig. 1), where lower temperature plasma is needed for enhancement of the negative ion production.[5] Later, this phenomenon was studied also experimentally[9–15] and theoretically[15–24] by several researchers.

Several different mechanisms have been proposed in literature for the explanation of the lower electron temperature beyond the filter. The most likely of them could be summarized as follows:

For low pressure (less than 1 Pa) dense plasmas with density in the order of 10^{17} m^{-3} or higher, the electron elastic collisions are dominated by the Coulomb collisions. Because of the strong energy dependence ($\nu_{e-i} \propto \varepsilon_e^{-3/2}$) of the Coulomb collision frequency (and particularly the electron-ion collisions frequency ν_{e-i}: the diffusion across the magnetic field due to electron-electron collisions is expected to be negligible[25]), the low-energy electrons have higher diffusion coefficient in the filter $D_\perp \propto D_\parallel (\nu_{e-i}/\omega_{ce})^2 \propto \nu_{e-i}/B^2$ compared to the high-energy electrons and therefore the low-energy electrons diffuse faster in the filter.[8,15,16] In the latter expressions ε_e is the electron energy, $\omega_{ce}=eB/m_e$ is the electron cyclotron frequency, e—the elementary charge, m_e—the electron mass, B—the magnetic field strength and $D_\parallel$ is the electron diffusion coefficient without magnetic field or along the magnetic field lines.

Another purely collisional mechanism, which could be responsible for the electron temperature reduction in the downstream region, is based on the fact that the electrons in the filter are strongly magnetized and the Larmor radius is much smaller than the filter size. Therefore, the time of flight of the electrons from the upstream to the downstream zone is

[a]Author to whom correspondence should be addressed. Also at Faculty of Physics, Sofia University, 5 James Bourchier Blvd., BG-1164 Sofia, Bulgaria. Telephone: 00 359 2 8161 643. Fax: 00 359 2 9625 276. Electronic mail: skolev@phys.uni-sofia.bg.

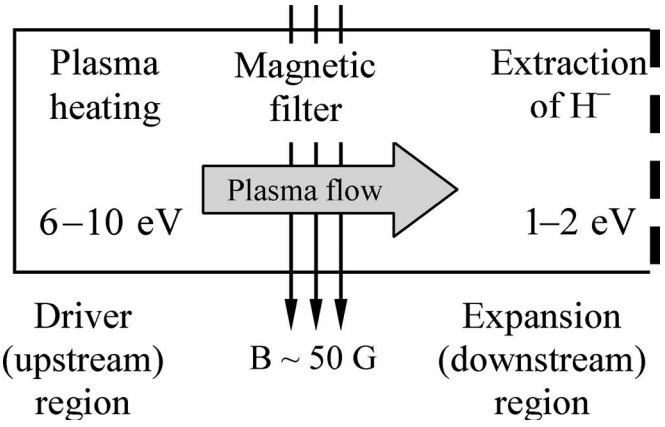

FIG. 1. Schematic representation of magnetic filtering in negative ion source.

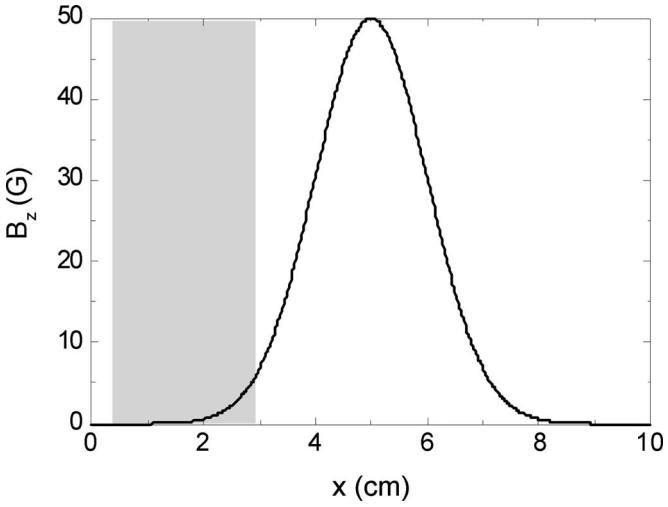

FIG. 2. Magnetic field profile (reference case $B_{z0}=50$ G) and particle injection and Maxwellization zone (gray area).

increased considerably and they need a lot of collisions in order to diffuse in the downstream region. As a consequence, during that passage, they lose significant part of their energy in inelastic and partially elastic collisions with neutrals and the electron temperature is reduced.

In Refs. 9 and 17–19 based on results from particle-in-cell (PIC) simulations, the energy selective transport of electrons across the filter is attributed to "turbulent" (also called "anomalous") transport. The electrons cross the filter due to $\tilde{E}\times B$ drift, where $\tilde{E}$ is low frequency oscillating electric field directed perpendicularly to the static filter field (B) and the plasma flow direction. The oscillating field $\tilde{E}$ is produced by excited instabilities due to the large differences in the plasma parameters from both sides of the filter. The high-energy electrons are supposed to diffuse slower across the filter than the low-energy ones because they "average out the fine scale fluctuations of the electric field."[18]

The purpose of this paper is to study the electron and negative ion transport in the magnetic filter by means of kinetic PIC with Monte Carlo collisions (PIC-MCCs) model with proper account for the collisional processes for several different cases. First we will discuss the electron transport across the magnetic filter without negative ions and for boundary conditions of grounded walls. Then we will show the effect of the magnetic filter on the basic plasma parameters for plasma with negative ions for various values of the magnetic field strength and applied bias potential at the wall in the downstream region.

II. NUMERICAL MODEL

A. Formulation of the problem

We consider a hydrogen plasma in one-dimensional (1D) domain with conducting walls at $x=0$ and $x=L$, where $L=10$ cm is the domain length. We assume infinity in the other directions y and z and plasma parameters varying only along x axis.

The magnetic filter is directed along the z axis $[\mathbf{B}=(0,0,B_z)]$ with Gaussian profile of the B_z component along x, centered in the middle of the domain (Fig. 2):

$$B_z(x) = B_{z0}\exp\left[-\frac{(x-x_0)^2}{2\sigma_B^2}\right], \tag{1}$$

where $x_0=5$ cm, $\sigma_B=1$ cm, and B_{z0} is varied in the simulations in the range of 0–70 G. This value of the magnetic field strength is high enough to magnetize the electrons [electron mean free path (mfp) 20 cm and Larmor radius larger than 1.5 mm] but does not affect significantly the ion motion and the ions remain unmagnetized: the ion's mfp is less than 5 mm and the Larmor radii are larger than 30 mm.

B. Particle-in-cell/Monte Carlo collisions model

The kinetic description of the described configuration is accomplished by means of the PIC method combined with MCCs. The PIC method[26] allows for the solution of the Vlasov–Poisson system by representing the distribution function of the different species as a collection of macroparticles in the phase space, which interact with electromagnetic fields created by themselves as well as those externally imposed. Initially (at time $t=0$) the particles are given within an initial distribution and the time evolution of the system is obtained by solving Newton's equations for each particle and the Poisson equation. The model presented here is 1D in the configuration space and three dimensional in velocity space ($1d$-$3v$) and the equations solved are

$$\frac{dx_\alpha}{dt} = v_{\alpha x}, \tag{2}$$

$$\frac{dv_\alpha}{dt} = \frac{q_\alpha}{m_\alpha}(\mathbf{E}+\mathbf{v}_\alpha\times\mathbf{B}), \tag{3}$$

where $\mathbf{v}_\alpha$ is the (type α) particle velocity vector, q_α—particle charge, m_α the particle mass and $\mathbf{E}$—the electric field vector. After the particle displacement, their charge is assigned to the grid nodes and the Poisson equation is solved to find the new values of the electric field which will be used in the next particle push. This cycle is repeated until steady state is reached. The charged particles considered here are electrons

TABLE I. Electron collision processes.

Reaction number	Process	Reference
1	$e+H \rightarrow e+H$ (elastic)	30 and 31
2	$e+H \rightarrow e+H^*$ (three energy levels)	32
3	$e+H \rightarrow 2e+H^+$	32
4	$e+H_2 \rightarrow e+H_2$	33
5	$e+H_2 \rightarrow e+H_2^*$ (17 energy levels)	32–36
6	$e+H_2 \rightarrow 2e+H_2^+$	32
7	$e+H_2 \rightarrow 2e+H^++H$	33
8	$e+H_2(v>3) \rightarrow H+H^-$	37
9	$e+H_2^+ \rightarrow H+H$	32
10	$e+H_2^+ \rightarrow e+H^++H$	32
11	$e+H_3^+ \rightarrow H_2+H$	32
12	$e+H_3^+ \rightarrow 3H$	32
13	$e+H_3^+ \rightarrow e+H^++2H$	32
14	$e+H_3^+ \rightarrow e+H^++H_2$	32
15	$e+H^- \rightarrow 2e+H$	32

e, three types of positive hydrogen ions H^+, H_2^+, H_3^+, and negative ions H^-. Thus the Poisson equation we solve is

$$\frac{d\Phi}{dx} = -\frac{e}{\varepsilon_0}(n_{H+} + n_{H2+} + n_{H3+} - n_e - n_{H-}), \tag{4}$$

where Φ is the electric potential, ε_0 is the vacuum permittivity, n_e is the electron density, n_{H-} is the H^- density, and n_{H+}, n_{H2+}, and n_{H3+}—the densities of H^+, H_2^+, and H_3^+ ions, respectively.

Collisions are incorporated in the model by using the Monte Carlo technique[27–29] provided that the time step is much smaller than the particles mean free time (mfp divided by mean speed of the particles).[29] For our conditions this is fulfilled and the MCC module is executed every time step in the PIC cycle. All the collision processes taken into account in the model are listed in Tables I and II.

The electrons collide primarily with hydrogen atoms and molecules but also some interactions with the ions are considered (Table I). The negative ions are produced by purely volume processes and particularly by dissociative attachment (No. 8 in Table I). The cross section used[37] is an effective cross section for the dissociative attachment of electrons with molecules excited to vibrational levels higher then 3 $[H_2(v>3)]$. The density of $H_2(v>3)$ is assumed to be proportional to the ground level molecules $H_2(v=0)$. Although this approach does not give precise values of the volume produced negative ion density it is completely sufficient for our purposes. Here we want to study the effects of the filter on electron and negative ion transport and we do not look for optimal conditions for maximum volume production of negative ions. The latter will require a detailed balance of the population of the vibrational levels which is out of the scope of this work. For such studies the reader is referred to Refs. 41 and 42.

TABLE II. Heavy particle collision processes.

Reaction number	Process	Reference
16	$H^++H \rightarrow H+H^+$ (charge exchange)	38
17	$H^++H \rightarrow H^++H$ (elastic)	38
18	$H^++H_2 \rightarrow H^++H_2$ (elastic)	39
19	$H^++H_2 \rightarrow H_2^++H$ (charge exchange)	39
20	$H_2^++H_2 \rightarrow H_2+H_2^+$ (charge exchange)	39
21	$H_2^++H_2 \rightarrow H_3^++H$	39
22	$H_3^++H_2 \rightarrow H_3^++H_2$ (elastic)	39
23	$H^-+H \rightarrow e+2H$	32
24	$H^-+H \rightarrow e+H_2^*$	32
25	$H^-+H \rightarrow H+H^-$ (charge exchange)	32
26	$H^-+H_2 \rightarrow H^-+H_2$ (elastic)	40
27	$H^-+H_2 \rightarrow e+H+H_2$	32
28	$H^++H^- \rightarrow H+H^*$	32
29	$H^++H^- \rightarrow e+H_2^+$	32

Several processes for negative ion losses are considered (processes 15, 23, 24, 27, 28, and 29 in Tables I and II) but for our conditions the predominant ones are the electron detachment due to atom impact (23 and 24).

Few of the processes listed in Tables I and II have a negligible contribution, but we keep them because in the different simulations the plasma parameters vary considerably and at certain conditions they may play certain role. The MC module takes little time compared to the PIC part and does not increase significantly the simulation time.

In order to keep the model as general as possible, we specify no particular type of discharge. Instead, the plasma is sustained by Maxwellization (explained below) of the electrons and injection of constant number of charged particles in the upstream region. Although in this way the simulation is not completely self-consistent, this approach allows us to impose the electron temperature in the upstream region which facilitates the comparison of the different cases considered here. The particles are injected and Maxwellized in the upstream zone (Fig. 2—gray zone). They are injected by pairs—electron and positive ion and there is no net charge introduced in the system. The Maxwellization of the electrons is done by virtual "Maxwellizing collisions" which lead to velocity Maxwellization. Every time step certain constant number of electrons are picked up (5.4×10^{20} physical particles per second for all simulations) depending on spatial profile of a collision probability we impose, and their velocity is changed by randomly sampling Maxwellian distribution with temperature T_M. Therefore the electron temperature in the upstream region never becomes exactly T_M but a bit lower (Fig. 4) because there are always particles which are not Maxwellized several time steps. Even if we increase significantly the rate of Maxwellizing collisions the only consequence will be the fact that the electron temperature in upstream region will be even closer to T_M. This approach of injection and heating of bounded plasma in the domain was chosen instead injection of particle flux from one of the walls in order to avoid the establishment of spurious potential structures near the injection plane and to obtain a potential profile consistent with the electron temperature which plays an important role for the particle transport across the magnetic filter. The boundaries are assumed to be completely absorbing.

TABLE III. External simulation parameters.

Description	Symbol	Value
Domain length	L	10 cm
Gas pressure	p	0.3 Pa
Gas temperature.	T_g	1000 K
Atom to molecule densities ratio	N_H/N_{H_2}	0.2
Densities ratio of vibrationally excited to ground state hydrogen molecules	$N_{H_2(v>3)}/N_{H_2(v=0)}$	0.01
Charged particles injection ratio	$e:H^+:H_2^+:H_3^+$	1:0.2:0.6:0.2
Maxwellization temperature	T_M	6 eV
Maximum magnetic field	B_{z0}	0–70 G
Magnetic filter position	x_0	5 cm
Standard deviation	σ_B	1 cm
Upstream wall potential	Φ_1	0 V
Downstream wall potential	Φ_2	0–30 V

III. RESULTS AND DISCUSSION

The main external parameters required by the model are summarized and defined in Table III. The gas pressure (0.3 Pa) corresponds to the value required by the ITER project for the operation of the negative ion sources. The values of the gas temperature T_g, the neutral species densities ratio $N_{H_2(v>3)}/N_{H_2(v=0)}$ and the charged particles injection ratio are based on Ref. 43. The plasma density considered here is in the order of 1×10^{16} m^{-3} and it is at least one order of magnitude smaller than the typical values in real devices used as negative ion sources. The density is limited because of the very long computational time (few weeks for single processor applications) required for simulations of high density plasmas.

The obtained results are sampled at steady state of the simulation. Steady state is reached within 2×10^{-4} s and this time is determined by the slowest relaxation time which is found to be the diffusion of the electrons trough the filter. Without magnetic field the simulation time is determined by the processes of production and destruction of negative ions and steady state is reached within 1×10^{-4} s. The typical value of the time step is 1×10^{-11} s and the total number of macroparticles used in the simulation is usually in the order of 1.1×10^5. The grid spacing is kept always less than half of the Debye length and the number of grid cells is usually in the order of 1000.

A. Negative ion free plasma with grounded walls

The presentation of the obtained results starts with the most simplified case of a negative-ion-free plasma with grounded walls ($\Phi_1=\Phi_2=0$). The spatial profiles of the plasma density and electric potential are shown on Figs. 3(a) and 3(b), respectively. Without magnetic field both profiles have small maxima in the upstream region due to the particle injection and Maxwellization there. The introduction of magnetic filter in the middle of our domain leads to an increase in the plasma density in the upstream region [Fig. 3(a)]. This is due to the fact that, in both cases, we inject the same number of charged particles but in the presence of a transverse magnetic field the electron diffusion toward the downstream region (on the right side of the filter) and hence the electron losses there are dramatically reduced.

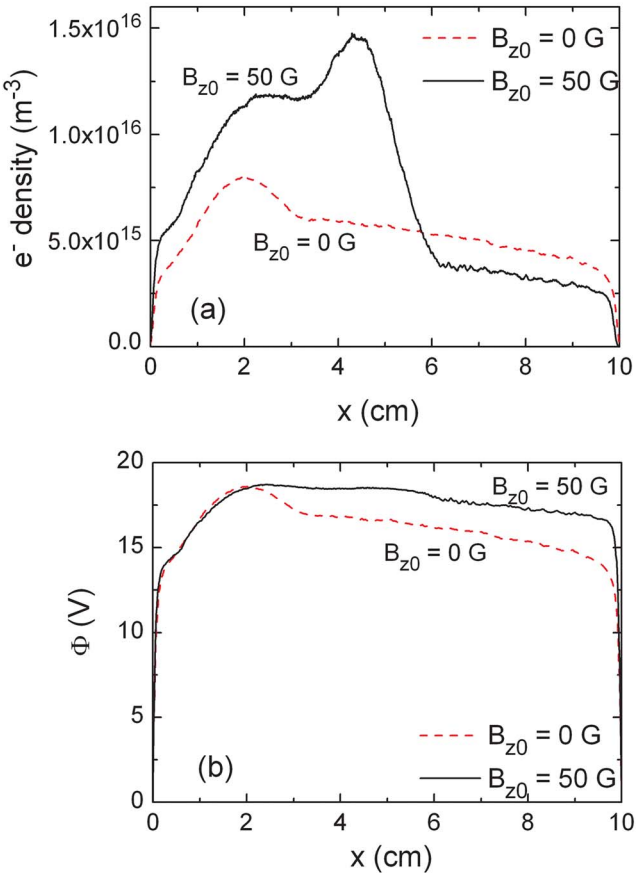

FIG. 3. (Color online) Electron density (a) and electric potential (b) spatial profiles with (B_{z0}=50 G, solid curves) and without magnetic filter (B_{z0}=0 G, dashed curves).

In the magnetic filter $[x\in(4-6)]$ the electrons are strongly magnetized ($\omega_{ce}/\nu_{e-n}>10^2$, where ν_{e-n} is the electron-neutral collision frequency in the order of 6×10^6 s^{-1}) and their Larmor radius does not exceed few millimeters. At these conditions the electrons need to collide many times in order to traverse the filter region[44] and they become stacked in the maximum magnetic field region for a very long time. As a result, there is accumulation of electrons and a maximum of the density in the filter [Fig. 3(a)]. This electron retention modifies the potential profile [Fig. 3(b)] and makes it flatter compared to the case without filter, in order to reduce the speed of the unmagnetized positive ions (ion mean free path 1—5 mm, minimum ion Larmor radius—40 mm) and to preserve the quasineutrality in the filter [Fig. 3(b)].

Without magnetic field, the electron mean free path (several centimeters) and thus the thermal conductivity are very high and the obtained electron temperature T_e is almost uniform in the volume (Fig. 4). The presence of magnetic field strongly reduces the energy transport across the filter and the electron temperature is significantly lowered in the downstream region.

The analysis of the obtained results gives an electron

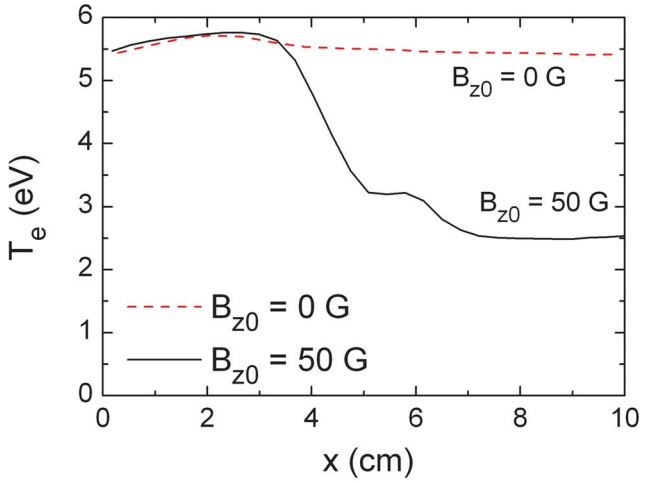

FIG. 4. (Color online) Electron temperature spatial profiles with (B_{z0}=50 G, solid curves) and without magnetic filter (B_{z0}=0 G, dashed curves).

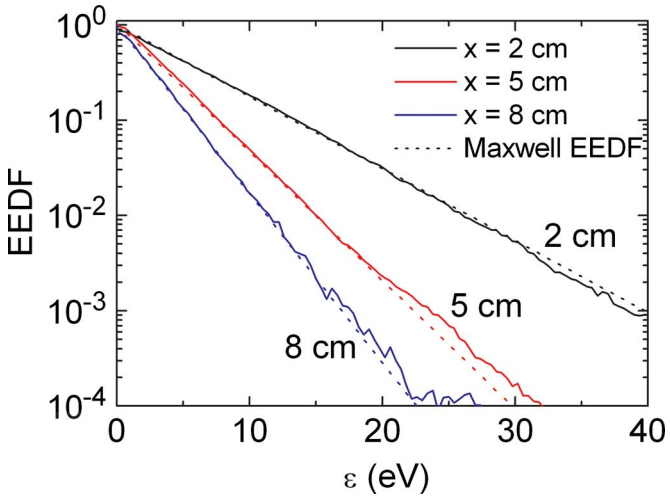

FIG. 5. (Color online) Normalized electron energy distribution function with magnetic filter (B_{z0}=50 G, solid curves) compared with Maxwellian EEDF (dashed curves) at different spatial positions as denoted on the figure. The Maxwellian EEDF is computed for T_e according to Fig. 4 at the corresponding position.

mean velocity (u_{ex}) across the filter, which is in rather good (within the statistical noise of the results) agreement with the classical drift-diffusion expression:[45]

$$u_{ex} = -\mu_\perp E_x - D_\perp \frac{1}{p_e}\frac{\partial p_e}{\partial x}, \tag{5}$$

where

$$\mu_\perp = \frac{\mu_\parallel}{1+\left(\frac{\omega_{ce}}{\nu_{e-n}}\right)^2} = \frac{e}{m_e \nu_{e-n}} \frac{1}{1+\left(\frac{\omega_{ce}}{\nu_{e-n}}\right)^2}, \tag{6a}$$

$$D_\perp = \frac{D_\parallel}{1+\left(\frac{\omega_{ce}}{\nu_{e-n}}\right)^2} = \frac{\kappa T_e}{m_e \nu_{e-n}} \frac{1}{1+\left(\frac{\omega_{ce}}{\nu_{e-n}}\right)^2} \tag{6b}$$

are, respectively, the mobility and the diffusion coefficient perpendicularly to the magnetic field, $\mu_\parallel = e/m_e\nu_{e-n}$ and $D_\parallel = \kappa T_e/m_e\nu_{e-n}$ are the mobility and the diffusion coefficient along (without) the magnetic field, $p_e = n_e \kappa T_e$ is the electron pressure and κ is the Boltzmann constant. This means that the electrons move in the direction perpendicular to the magnetic field only due to collisions with neutrals. Examination of separate particles trajectories confirms that. The electrons need large number of collisions (in the order of several hundreds) in order to traverse from the upstream to the downstream region. Most of these collisions are elastic but among them a few inelastic collision also appear and they are enough to cause significant energy loss and decrease in the averaged energy and thus T_e (Fig. 4). This suggests that there is no a real "energy selective" transport of the electrons trough the filter but instead all "types" of electrons (with arbitrary energy) are allowed to enter and cross the filter but will exit with significantly reduced energy.

However we should emphasize that this conclusion is strictly true only for plasmas with weak influence of the Coulomb collisions ($\nu_{e-n}/\nu_{e-i} \gg 1$, where ν_{e-i} is the collision frequency for Coulomb collisions). For high density ($n_e > 10^{17}$ m^{-3}) and low pressure plasma ($p < 1$ Pa) this is not fulfilled and the strong energy dependence of ν_{e-i} ($\nu_{e-i} \propto \varepsilon_e^{-3/2}$) may modify the transport properties. In this case the electron energy reduction due to inelastic and partially elastic collisions will be in competition with energy selective transport due to Coulomb collisions. These effects will be studied in a future work.

It is worth noting that drift instabilities in the $\tilde{E}\times B$ direction can also enhance electron transport in the direction of the applied electric field. This mechanism was discussed in Refs. 17–19 and was found to play an important role in electron transport in these references because classical transport due to collisions was not present (collisionless PIC simulation). In any case, transport in the $\tilde{E}\times B$ direction certainly has some influence on plasma uniformity and on the plasma flow across the magnetic field and we plan to include it in future work by means of a $2d$-$3v$ PIC-MCC model.

Figure 5 shows the spatial evolution of the normalized electron energy distribution function (EEDF). We remind that the distribution function in the upstream region (position 2 cm in Fig. 5) is imposed to be Maxwellian with temperature 6 eV. From these results we find that the EEDF shape is not significantly affected by the magnetic filter and it is preserved Maxwellian in the whole domain.

It is worth to notice at that point that the presented results are in qualitative agreement with results from fluid modeling[24] of the problem. Similar accumulation of electrons in the filter and similar behavior of the electron temperature are observed. However, this is not surprising if we keep in mind the collisional nature of the electron and ion transport across the filter, which is properly resolved by the fluid models.

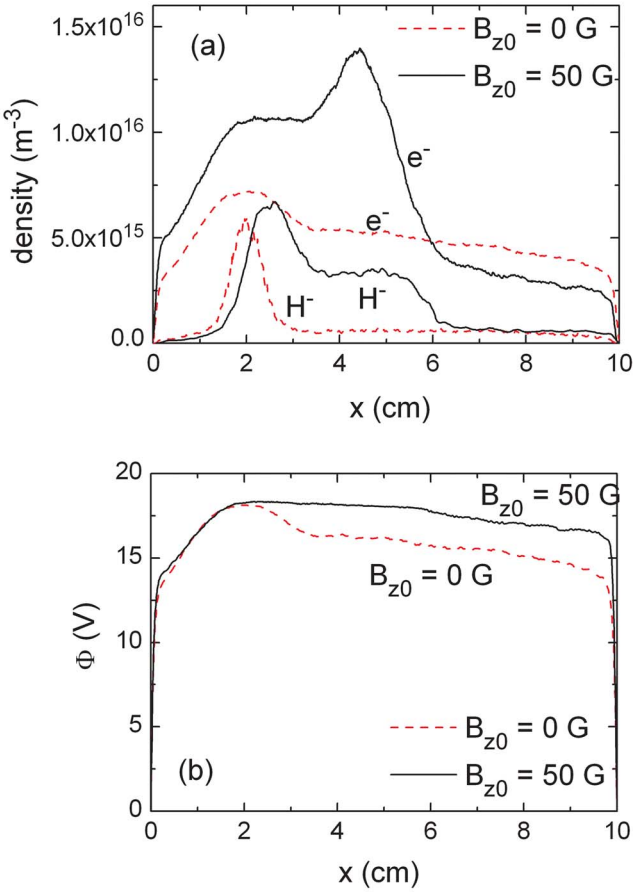

FIG. 6. (Color online) Electron and H^- densities (a) and electric potential (b) spatial profiles with (B_{z0}=50 G, solid curves) and without magnetic filter (B_{z0}=0 G, dashed curves).

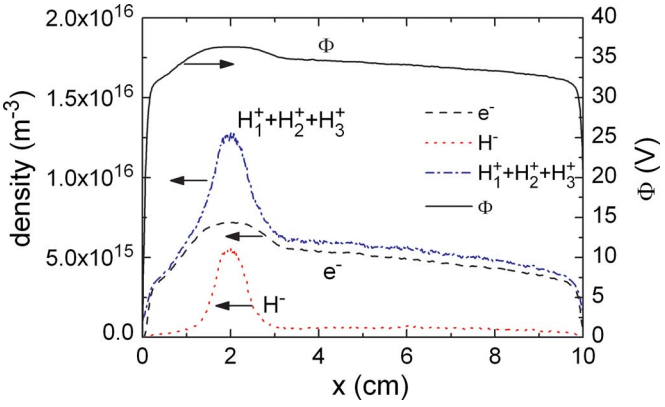

FIG. 7. (Color online) Electron (e^-), negative ion (H^-) and sum of positive ions (H^++H_2^++H_3^+) densities as well as electric potential (Φ) profile for bias potential of Φ_2=20 V and no magnetic filter (B_{z0}=0 G).

B. Electronegative plasma with negative ion "extraction"

Here, we consider weakly electronegative plasma with magnetic filter and extraction of the negative ions by application of different bias voltages (Φ_2) on the wall in the downstream region.

Figure 6 presents the influence of the negative ions on the plasma parameters for the conditions of grounded walls (no extraction). The electron density and the potential without magnetic field are, in practice, not affected by the presence of negative ions due to the low plasma electronegativity and remain basically the same as in Fig. 3. The well pronounced maximum in the potential without magnetic field [Fig. 6(b)] strongly concentrates the negative ions there. However, this is not the case with magnetic filter. In this case there is a wide region with almost constant potential and thus the negative ions are spread in the region of 2–6 cm. The higher number of negative ions with filter [Fig. 6(a)] is due to the increased production as a consequence of higher electron density.

In both cases the H^- ions reside in a potential well and because of their low energy, they cannot overcome the wall sheath and reach the walls. At these conditions they are produced and lost only in volume processes. In order to extract them we must apply a positive potential equal or higher than the plasma potential. Figure 7 shows the result of an attempt at extracting H^- ions without magnetic filter and bias voltage of 20 V, which is slightly higher than the plasma potential. The result is just a shift up of the potential with the bias voltage and there is no any modification of the density profiles (Fig. 7). The negative ions are still in a potential well and are concentrated at the peak of the potential and thus they could not be extracted. This behavior is straightforwardly explained if we keep in mind that the considered plasma is weakly negative and the plasma potential is still determined by electron temperature. The introduction of positive bias (attracting for the electrons and H^-) increases the electron losses and the potential profiles adapts itself in order to preserve the quasineutrality in the system and to assure equal fluxes of negative and positive species in total to the walls.

By introducing transverse magnetic field, the electron losses on the biased wall in the downstream region are significantly reduced and the potential tends [Fig. 8(a)] to the value corresponding to the conditions of grounded walls and thus determined by the electron temperature (imposed in our model) in the upstream region. Magnetic field with B_{z0}=20 G is enough to make the electron losses on the biased wall negligible compare to the upstream region and thus to exclude them as a factor determining the plasma potential [Fig. 8(a)]. In the presence of magnetic field the number of electrons crossing the filter and reaching the downstream region is relatively small and because of the lack of wall sheath [Fig. 8(a), B_{0z}=50 G] near the biased (Φ_2=20 V) wall, they are quickly lost on the wall and the electron density in this region becomes negligible [Fig. 8(b)]. At these conditions the electric field accelerates the unmagnetized H^- ions toward the biased wall and an electronegative plasma is established in the downstream region—the quasineutrality is ensured by the negative and positive ions [Fig. 8(b)].

Because of the negligible electron density in the downstream region [Fig. 8(b)] the negative ion production there becomes negligible and the extracted negative ions are mainly produced in the upstream and the filter regions. This observation raises the question whether similar configuration is optimal for volume based production of negative ions. It is

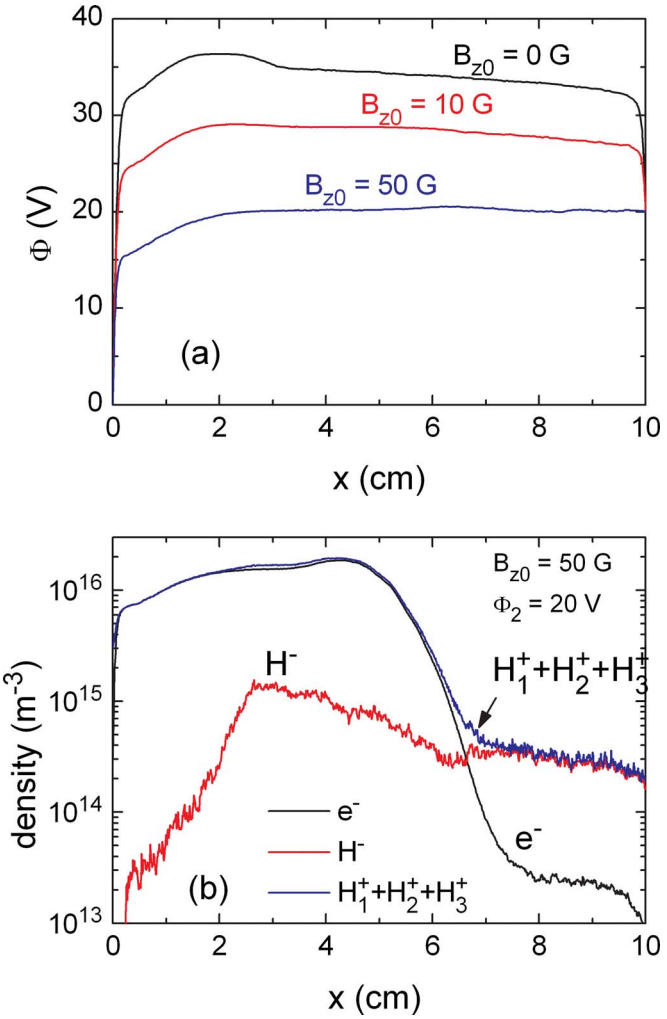

FIG. 8. (Color online) (a) Electric potential spatial profiles for different magnetic field strength and bias voltage of Φ_2=20 V; (b) electron (e^-), negative ion (H^-) and sum of positive ions (H^++H_2^++H_3^+) densities for bias potential of Φ_2=20 V and magnetic filter with (B_{z0}=50 G).

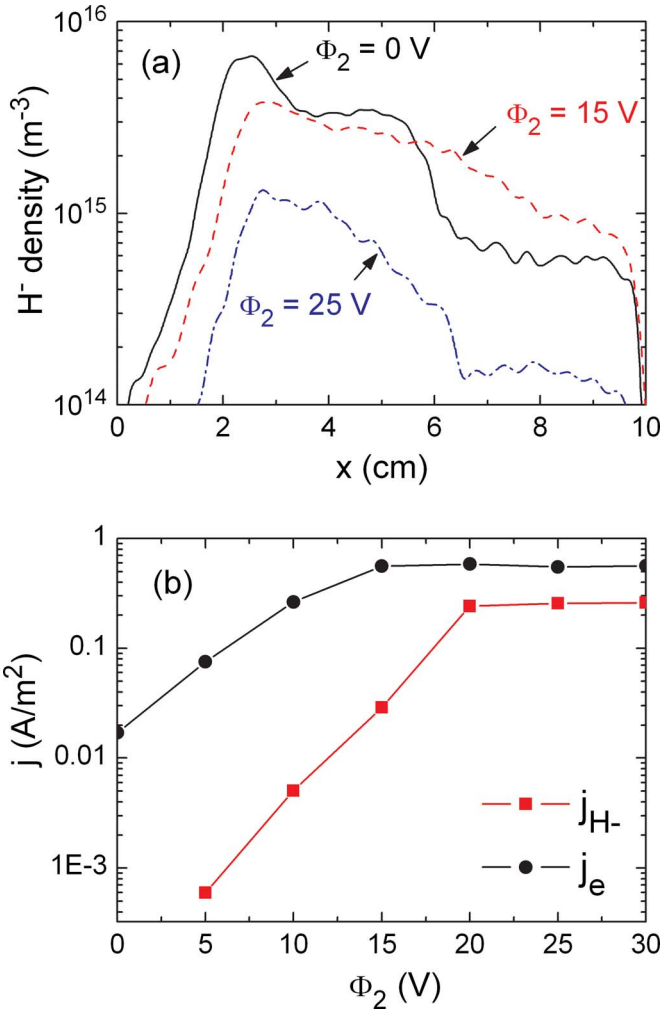

FIG. 9. (Color online) (a) Negative ion density profiles for different bias potentials and B_{z0}=50 G; (b) extracted H^- and electron currents at the wall in the downstream region (x=10 cm) as a function the bias potential Φ_2 for B_{z0}=50 G.

widely accepted that the most efficient channel for volume based[5] negative ion productions is the two step process: (1) vibrational excitation of hydrogen molecules to high vibrational levels and (2) dissociative attachment (process 8 in Table I). Based on that, the "tandem" type of negative ion source was proposed where the source is divided by a magnetic filter into two parts: "hot" part with high electron temperature for efficient vibrational excitation and "cold" part with low T_e, which enhances the dissociative attachment process having maximum cross section near 1 eV. In our configuration, this scheme is not very effective because the depletion of electrons in the downstream region does not allow the H^- production there and the ions are produced only in the hot part of the source. However such behavior will not affect the rate of possible surface production of H^-,[3,6] which is based on interaction of heavy particles with the wall.

The H^- ions density evolution for different bias voltages can be seen on Fig. 9(a). With the increase of Φ_2 the potential profile becomes flatter and for $\Phi_2 \geq 20$ V the electric field in the plasma interior [Fig. 8(a)] attracts the H^- ions toward the wall in the downstream region. This considerably modifies the density profiles [Fig. 9(a)]. For low bias voltages $\Phi_2 \in (0-15)$ V the H^- density in the downstream region increases, but for higher Φ_2 the H^- density decreases in the whole domain [Fig. 9(a), Φ_2=25 V] due to the faster extraction (ion acceleration toward the biased wall) and the limited H^- production (the electron density in the upstream and filter regions changes slightly with Φ_2).

By varying the bias potential Φ_2 we can build a current-voltage characteristic of the extracted H^- and electron currents [Fig. 9(b)]. The result resembles a probe characteristic: the negative ion and electron currents have an exponential increase up to the plasma potential and saturate for higher values of the bias potential. The negative ion saturation current is limited and determined by the diffusion speed of negative ions from the upstream to the downstream region. When the bias becomes higher than the plasma potential ($\Phi_2 \geq 20$ V in our case) the plasma potential profile in the upstream region remains the same and the potential difference between the biased wall and the plasma potential in the upstream region is compensated (screened) within the downstream region. The density profiles upstream stay nearly con-

stant and hence a constant number of H^- ions is produced. Therefore the negative ion flux coming from the upstream and the filter areas (where H^- are produced) remain the same and determined by the density gradient and the weak electric field in the filter. The volume losses of H^- in the downstream only slightly reduce the current toward the biased wall. The electron saturation current is determined by the limited electron diffusion trough the magnetic filter. The negative ion to electron current ratio at the saturation section ($\Phi_2 \geq 20$ V) is found to be 0.41.

IV. CONCLUSION

We have presented in this paper a kinetic simulation of hydrogen plasma with localized transverse magnetic field (magnetic filter). The electron and negative ion transport across the filter was analyzed and the obtained results suggest that for the considered conditions (plasma densities of 10^{16} m^{-3} and pressure of 0.3 Pa) the primary effect of the filter on the electrons is the increase in the number of collisions the electrons need in order to diffuse from the upstream to downstream region. As a result, more inelastic collisions appear and the electron energy and thus the electron temperature are significantly reduced. That is why there is no a preferential transport of the low-energy compared to the high-energy electrons in the filter, but just a substantial energy loss for all the electrons.

Although this model could not represent exactly the extraction physics of the negative ions, it still gives us important results for the physical processes between the extraction system and the magnetic filter. The combination of a magnetic filter and a positive applied bias (extraction) voltage leads not only to electron temperature reduction in the expansion region but also to depletion of electrons and establishment of electronegative plasma in the downstream region. This effect reduces the H^- destruction due electron impact but also reduces the H^- production through volume processes and thus the extracted ions are produced in the hot part of the source—the upstream region. It seems that such a configuration with small electron density near the extraction system is more favorable for surface processes based H^- production[3,6] than for volume based production.

The extraction of the negative ions becomes feasible when we apply high enough magnetic field in order to reduce the electron losses (the plasma screening) and high enough bias potential (higher than the upstream plasma potential) in order to remove the potential barrier (the wall sheath) near the extraction electrode and to allow the ions to reach it.

The current work is limited to a 1D configuration and does not consider possible two-dimensional (2D) effects like additional ambipolar fields induced by $\mathbf{E} \times \mathbf{B}$ drifts and drifts in direction of the plasma flow due to oscillating electric fields in direction perpendicular to plasma flow. Therefore, the simulations will be extended in the future toward more realistic 2D configurations.

ACKNOWLEDGMENTS

This work has been supported by the EURATOM/CEA and by the Federation Nationale de Recherche Fusion par Confinement Magnétique-ITER. S.K. benefited from a CNRS postdoctoral fellowship.

[1] *ITER Technical Basis 2002, ITER EDA Documentation Series No. 24* (IAEA, Vienna, 2001).
[2] H. W. Loeb, Plasma Phys. Controlled Fusion **47**, B565 (2005).
[3] R. S. Hemsworth and T. Inoue, IEEE Trans. Plasma Sci. **33**, 1799 (2005).
[4] U. Fantz, P. Franzen, W. Kraus, H. D. Falter, M. Berger, S. Christ-Koch, M. Fröschle, R. Gutser, B. Heinemann, C. Martens, P. McNeely, R. Riedl, E. Speth, and D. Wünderlich, Rev. Sci. Instrum. **79**, 02A511 (2008).
[5] M. Bacal, A. Hatayama, and J. Peters, IEEE Trans. Plasma Sci. **33**, 1845 (2005).
[6] M. Bacal, Nucl. Fusion **46**, S250 (2006).
[7] K. N. Leung, K. W. Ehlers, and M. Bacal, Rev. Sci. Instrum. **54**, 56 (1983).
[8] A. J. T. Holmes, Rev. Sci. Instrum. **53**, 1517 (1982).
[9] O. Fukumasa, H. Naitou, and S. Sakiyama, J. Appl. Phys. **74**, 848 (1993).
[10] O. Fukumasa, M. Hosoda, and H. Naitou, Rev. Sci. Instrum. **63**, 2696 (1992).
[11] K. N. Leung, O. Anderson, C. Chan, W. Cooper, G. DeVries, C. Hauck, W. Kunkel, J. Kwan, A. Lietzke, P. Purgalis, and R. Wells, Rev. Sci. Instrum. **61**, 2378 (1990).
[12] T. A. Santhosh Kumar, S. K. Mattoo, and R. Jha, Phys. Plasmas **9**, 2946 (2002).
[13] I. Djermanov, St. Kolev, St. Lishev, A. Shivarova, and Ts. Tsankov, J. Phys.: Conf. Ser. **63**, 012021 (2007).
[14] Q. Al-Jibouri, A. J. T. Holmes, and W. G. Graham, Plasma Sources Sci. Technol. **5**, 401 (1996).
[15] F. A. Haas, L. M. Lea, and A. J. T. Holmes, J. Phys. D: Appl. Phys. **24**, 1541 (1991).
[16] A. J. T. Holmes, Plasma Sources Sci. Technol. **5**, 453 (1996).
[17] H. Naitou, K. Ohi, and O. Fukumasa, Rev. Sci. Instrum. **71**, 875 (2000).
[18] K. Ohi, H. Naitou, Y. Tauchi, and O. Fukumasa, Phys. Plasmas **8**, 23 (2001).
[19] K. Ohi, H. Naitou, Y. Tauchi, and O. Fukumasa, Plasma Phys. Controlled Fusion **43**, 1615 (2001).
[20] M. Shirai, M. Ogasawara, T. Koishimine, and A. Hatayama, Rev. Sci. Instrum. **67**, 1085 (1996).
[21] A. Fukano and M. Ogasawara, Jpn. J. Appl. Phys., Part 1 **40**, 7072 (2001).
[22] T. Sakurabayashi, A. Hatayama, and M. Bacal, Rev. Sci. Instrum. **75**, 1770 (2004).
[23] T. Mizuno, Y. Kitade, A. Hatayama, T. Sakurabayashi, N. Imai, T. Morishita, and T. Inoue, Rev. Sci. Instrum. **75**, 1760 (2004).
[24] St. Kolev, St. Lishev, Kh. Tarnev, and R. Wilhelm, Plasma Phys. Controlled Fusion **49**, 1349 (2007).
[25] M. N. Rosenbluth and A. N. Kaufman, Phys. Rev. **109**, 1 (1958).
[26] C. K. Birdsall and A. B. Langdon, *Plasma Physics via Computer Simulation* (McGraw-Hill, New York, 1985).
[27] C. K. Birdsall, IEEE Trans. Plasma Sci. **19**, 65 (1991).
[28] V. Vahedi and M. Surendra, Comput. Phys. Commun. **87**, 179 (1995).
[29] K. Nanbu, IEEE Trans. Plasma Sci. **28**, 971 (2000).
[30] Y. Itikawa, At. Data Nucl. Data Tables **14**, 1 (1974).
[31] S. Trajmar and I. Kanik, in *Atomic and Molecular Processes in Fusion Edge Plasmas*, edited by R. K. Janev (Plenum, New York, 1995), p. 40.
[32] R. K. Janev, D. Reiter, and U. Samm, "Collision processes in low-temperature hydrogen plasmas," FZ-Jülich Report No. 4105, 2003, available at http://www.eirene.de/report_4105.pdf.
[33] S. J. Buckman and A. V. Phelps, J. Chem. Phys. **82**, 4999 (1985).
[34] J. Yoon, M. Song, J. Han, S. Hwang, W. Chang, B. Lee, and Y. Itikawa, J. Phys. Chem. Ref. Data **37**, 913 (2008).
[35] H. Ehrhardt, L. Langhans, F. Linder, and H. S. Taylor, Phys. Rev. **173**, 222 (1968).
[36] S. J. Buckman and A. V. Phelps, JILA Information Center Report No. 27, University of Colorado, 1 May 1985, data available at http://jilawww.colorado.edu/~avp/collision_data/electronneutral.
[37] R. K. Janev, W. D. Langer, K. Evans, Jr., and D. F. Post, Jr., *Elementary Processes in Hydrogen-Helium Plasmas* (Springer, Berlin, 1987).

[38]P. S. Krstić and D. R. Schultz, *Atomic and Plasma-Material Interaction Data for Fusion 8* (IAEA, Vienna, 1998).
[39]A. V. Phelps, personal communication (19 April 2008).
[40]A. V. Phelps, J. Phys. Chem. Ref. Data **19**, 653 (1990).
[41]Ts. Paunska, H. Schlüter, A. Shivarova, and Kh. Tarnev, Phys. Plasmas **13**, 023504 (2006).
[42]M. Capitelli, M. Cacciatore, R. Celiberto, O. De Pascale, P. Diomede, F. Esposito, A. Gicquel, C. Gorse, K. Hassouni, A. Laricchiuta, S. Longo, D. Pagano, and M. Rutigliano, Nucl. Fusion **46**, S260 (2006).
[43]U. Fantz, personal communication (15 July 2008).
[44]F. Chen, *Introduction to Plasma Physics and Controlled Fusion* (Plenum, New York, 1984).
[45]M. A. Lieberman and A. J. Lichtenberg, *Principles of Plasma Discharges and Materials Processing* (Wiley, New York, 1994).